

Communication

Effect of Surface Nonlinearity Distribution on Second Harmonic Generation under Tightly Focused Beams

Sergey Scherbak^{1,2}, Ilya Reshetov^{1,2}, Gennadiy Kan¹ and Andrey Lipovskii^{1,2,*} 

¹ Department of Physics and Technology of Nanoheterostructures, Alferov University, St. Petersburg 194021, Russia; sergeygtm@yandex.ru (S.S.); reshetov_iv@spbstu.ru (I.R.); kan@spbau.ru (G.K.)

² Laboratory of Multifunctional Glassy Materials, Peter the Great St. Petersburg Polytechnic University, St. Petersburg 195251, Russia

* Correspondence: lipovsky@spbau.ru

Abstract: A thorough integral formulation describing the second harmonic generation under tightly focused linearly and radially polarized beams for an arbitrary distribution of the nonlinear susceptibility over the surface of isotropic media was presented. We numerically simulated effects caused by the straight edge of the nonlinear region. In particular, we demonstrated that the second harmonic radiation in the normal direction, which is forbidden in common cases of highly symmetrical nonlinear surfaces, is allowed in the presence of the edge. This is provided by $\chi^{(2)}_{\text{zxz}}$ -component of the second-order susceptibility.

Keywords: optical second harmonic generation; radial polarization; tight focusing; edge effect

1. Introduction

Nonlinear optical phenomena have been studied for more than half a century after the discovery of the second harmonic generation (SHG) [1]. Since then, considerable interest has been attracted to the nonlinear properties of micro- [2] and nanosized metal [3] and dielectric [4] structures including surfaces of solids, which provide SHG even in the case of isotropic materials [5]. The latter is due to breaking their central symmetry at interfaces, while bulk isotropy nullifies the second-order nonlinear susceptibility of $\chi^{(2)}$ in an approximation of only dipolar nonlinear interactions [6]. Thus, second-order nonlinear optical phenomena are surface-specific for isotropic and centrosymmetric materials (if generally weak non-local bulk contributions that involve high-order multipole interactions are neglected). Because of this, they became a powerful tool for probing and sensing surfaces [7–10].

The most evident way to increase the second harmonic (SH) output is to use optical fields of high intensity. For small objects, this is possible in the regime of tight focusing of the fundamental radiation, when the size of a light spot is about the radiation wavelength. Besides, the nonlinear interaction can be additionally enhanced using resonant properties of nonlinear objects [11–13]. Nontrivially, polarized fundamental beams provide noticeably tighter focusing than trivially polarized ones [14]. Also, they enable highly localized measurements of nonlinearity, particularly, to analyze separately surface and bulk nonlinear responses [6]. Moreover, tightly focused radially polarized beams have a significant longitudinal component of the electric field near the focal plane. This allows the fundamental wave to interact particularly with $\chi^{(2)}_{\text{zzz}}$ component of the tensor of the second order susceptibility, dominating in many structures based on isotropic materials [15,16], even for normal (z-) incidence, which is not possible in conventional SHG schemes [17].

In recent decades, radially polarized beams became a powerful tool for analyzing the nonlinearity of micro- and nanoscaled objects. Particularly, studies of Mie-resonant nanoparticles [18] and metal nanostructures [19,20] were reported. Also, radial polarization was used for the analysis of spatially resolved SHG by centrosymmetric glasses [6] and nonlinear films [21]. Both semi-analytical [22] and fully-numerical [23] models of



Citation: Scherbak, S.; Reshetov, I.; Kan, G.; Lipovskii, A. Effect of Surface Nonlinearity Distribution on Second Harmonic Generation under Tightly Focused Beams. *Photonics* **2023**, *10*, 350. <https://doi.org/10.3390/photonics10040350>

Received: 1 March 2023

Revised: 18 March 2023

Accepted: 21 March 2023

Published: 23 March 2023



Copyright: © 2023 by the authors. Licensee MDPI, Basel, Switzerland. This article is an open access article distributed under the terms and conditions of the Creative Commons Attribution (CC BY) license (<https://creativecommons.org/licenses/by/4.0/>).

SHG, by a material with T_d -symmetry under radially polarized excitation, were reported, as well as a model of SHG by a centrosymmetric sphere under tightly focused linearly polarized excitation [24].

In our recent study [25] we theoretically described SHG by axially symmetric, C_{4v} - and C_{6v} -symmetric media, which have the same structure of $\chi^{(2)}$ tensor. Both surface and bulk responses were considered in [25], and analytical equations describing SH radiation patterns (RP) were derived. Using the model developed, we compared SHG by surface and bulk of axially symmetric media under both linearly and radially polarized excitations. Particularly, it has been shown that the bulk nonlinearity distributed within a few microns of depth (e.g., in the case of micron-thick nonlinear films or poled glasses [26]) demonstrates little difference from the purely surface one.

In the present study, we extend that model to the case of an arbitrary distribution of $\chi^{(2)}$ over the lateral (xy) plane. This allowed us to analyze the effect of the straight edge of the nonlinear region on the SH radiation and to declare it as a tool for additional control over the radiation. The latter can be provided by patterned films [27] or glasses poled with a profiled electrode [28,29]. We considered only $\chi^{(2)}_{zzz}$ and $\chi^{(2)}_{zxx}$ components. The former is presumably dominant and therefore is the most practically interesting one for poled glasses [16] and surfaces of isotropic/centrosymmetric materials [15,30,31]. The $\chi^{(2)}_{zxx}$ component, as we show here, provides SH radiation in the normal direction, a unique phenomenon in studies of SHG in highly symmetrical media.

2. Theory

We consider a light beam tightly focused on the nonlinear surface-interface between two media with indices n_1 and n_2 . The light propagates along the z -axis while the interface is normal to z . Here we follow the approach used in similar works [22,23,32] and in our paper [25]. The approach consists of the following subsequent steps. First, the distribution of the electric field of the fundamental light wave near the focal plane is to be calculated via Richards and Wolf’s integral formulation, which represents a superposition of plane waves propagating within the aperture angle of the lens [33,34]. Next, via nonlinear constitutive equations, which connect second-order polarization with quadratic combinations of components of the fundamental electric field, we calculate the distribution of the second-order polarization for given non-zero components of the nonlinear susceptibility $\chi^{(2)}$. Finally, using the standard expression for dipole radiation in the far-field zone, we describe the RP of the second harmonic generated by the calculated distribution of the nonlinear polarization.

The approach was described in detail elsewhere [25]. Here we provide the most necessary expressions and specify features originating from the distribution of optical nonlinearity over the interface.

The cartesian components of the electric field of the second harmonic wave in the far-field zone can be calculated as follows (see the scheme in Figure 1a):

$$E_x^{2\omega} = \int_0^{+\infty} r dr \int_0^{2\pi} d\varphi \left[\sin \theta_r \cos \varphi_r \left(P_x^{2\omega} \sin \theta_r \cos \varphi_r + P_y^{2\omega} \sin \theta_r \sin \varphi_r + P_z^{2\omega} \cos \theta_r \right) - P_x^{2\omega} \right] e^{-iKr \cos(\varphi - \varphi_r) \sin \theta_r}, \quad (1)$$

$$E_y^{2\omega} = \int_0^{+\infty} r dr \int_0^{2\pi} d\varphi \left[\sin \theta_r \sin \varphi_r \left(P_x^{2\omega} \sin \theta_r \cos \varphi_r + P_y^{2\omega} \sin \theta_r \sin \varphi_r + P_z^{2\omega} \cos \theta_r \right) - P_y^{2\omega} \right] e^{-iKr \cos(\varphi - \varphi_r) \sin \theta_r}, \quad (2)$$

$$E_z^{2\omega} = \int_0^{+\infty} r dr \int_0^{2\pi} d\varphi \left[\cos \theta_r \left(P_x^{2\omega} \sin \theta_r \cos \varphi_r + P_y^{2\omega} \sin \theta_r \sin \varphi_r + P_z^{2\omega} \cos \theta_r \right) - P_z^{2\omega} \right] e^{-iKr \cos(\varphi - \varphi_r) \sin \theta_r}. \quad (3)$$

$P_x^{2\omega}$, $P_y^{2\omega}$, and $P_z^{2\omega}$, here, are cartesian components of the induced second-order polarization, θ_r and φ_r are angles that define the direction of radiation, φ and r are cylindrical coordinates in the focal plane. Note, compared to the expressions presented in [25], in Equations (1)–(3) we omitted the constant factor $-e^{iK|\mathbf{R}|} \cdot (2\omega)^2 / c^2 |\mathbf{R}|$ (ω is the fundamen-

tal frequency, K is the SH wavenumber) and the integration over z , since here we limit our consideration only with the interface (surface) nonlinearity. In this study we consider a highly symmetrical nonlinear surface with the following non-zero components of $\chi^{(2)}$: $\chi^{(2)}_{zzz}, \chi^{(2)}_{zxx}, \chi^{(2)}_{xzx}$. As we mentioned in the Introduction, axially symmetric, C_{4v} - and C_{6v} -materials and surfaces of isotropic and centrosymmetric materials have this structure of $\chi^{(2)}$. Thus, the corresponding nonlinear constitutive equations in the case of radially polarized incoming fundamental wave are:

$$P_z^{2\omega} = \chi_{zzz}^{(2)} E_z^2 + \chi_{zxx}^{(2)} E_r^2. \tag{4}$$

$$P_y^{2\omega} = \chi_{xzx}^{(2)} E_z E_r \sin \varphi. \tag{5}$$

$$P_x^{2\omega} = \chi_{xzx}^{(2)} E_z E_r \cos \varphi. \tag{6}$$

For linear (x -) polarization these are:

$$P_z^{2\omega} = \chi_{zzz}^{(2)} E_z^2 + \chi_{zxx}^{(2)} E_x^2. \tag{7}$$

$$P_x^{2\omega} = \chi_{xzx}^{(2)} E_z E_x. \tag{8}$$

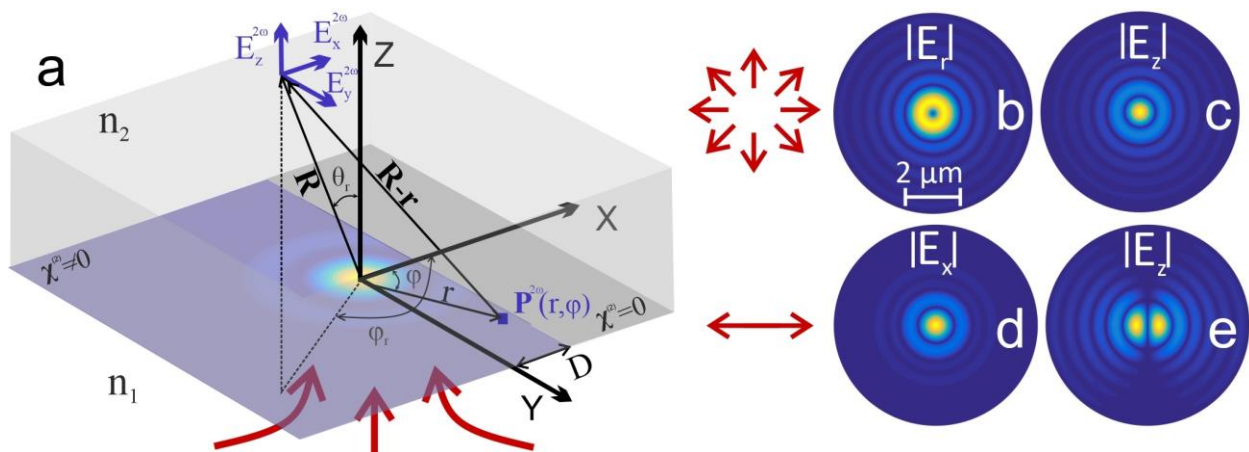


Figure 1. (a) Scheme of the problem; color map represents a typical $|P^{2\omega}|$ -distribution; D varies in our calculations; negative D corresponds to the beam center falling over the edge; the arrows indicate direction of excitation. Distributions of r - (b) and z -components (c) of E -field of the radially polarized fundamental wave and x - (d) and z -components (e) of E -field of the linearly (x -) polarized fundamental wave in the focal plane; the arrows schematically indicate polarization.

Expressions for distributions of the components of fundamental field (E_z, E_r for radial polarization, and E_z, E_x for linear polarization) are provided in Refs. [25,33,34]. The main difference with Ref. [25] is that here not only fundamental field has a certain distribution over the focal plane, but also an arbitrary distribution of surface nonlinear susceptibility $\chi^{(2)}$ is assumed. Further, we consider a straight edge of the nonlinear region. The scheme of the system under consideration is presented in Figure 1a. Distance D between the center of the focused fundamental beam and the edge of the nonlinear region of the surface was varied in the calculations. Negative D corresponds to the case when the beam center falls over the edge. The other parameters used in the calculations are: numerical aperture of the focusing lens $NA = 0.9$, fundamental wavelength $\lambda = 1064$ nm, $n_1 = 1.0$ (air), $n_2 = 1.51$ (typical glass), the beam is focused exactly at the surface, and an incoming fundamental wave is Bessel-Gauss beam of the lowest order with the waist at the plane of the pupil [25,33], the beam waist coincides with the pupil radius.

Because of the nonuniform distribution of $\chi^{(2)}$, the integration over φ in Equations (1)–(3) does not have an analytical representation and we calculated all the integrals numerically. The intensity of the SH wave in the far-field zone as a function of the radiation direction defined by angles θ_r and φ_r is proportional to a squared modulus of $E^{2\omega}$ -field:

$$I^{2\omega}(\theta_r, \varphi_r) \sim |E_x^{2\omega}|^2 + |E_y^{2\omega}|^2 + |E_z^{2\omega}|^2. \quad (9)$$

Also, to account for the refraction of the SH radiation at the rear side of the sample that is typically a flat plate (the interface $n_2 \rightarrow n_1$), we substituted refraction angle θ_r^2 for θ_r and multiplied Equation (9) by the Fresnel coefficient. The details can be found in [25].

3. Results and Discussion

3.1. $\chi^{(2)}_{zzz}$ -Component

In Figure 2, we present the results from the calculations for the radially polarized incoming fundamental wave in the case of a single non-zero $\chi^{(2)}_{zzz}$ -component of the second-order susceptibility. The upper panel of Figure 2 demonstrates the radial distribution of $|P_z^{2\omega}|$. The maximum value of the distribution is in the center of the beam which correlates with the features of the fundamental field distribution, particularly, with E_z (see Figure 1c). Thus, $P_z^{2\omega}$ is primarily distributed in the central bright spot with a radius of ~ 300 nm at the half-maximum level. According to the distribution of the fundamental E -field components presented in Figure 1b,c, the radius of the fundamental spot is about 300–400 nm. There is also an obscure outer ring in the distribution of $P_z^{2\omega}$, but its intensity does not exceed a few percent of the maximal (central) one. In the middle panel of Figure 2, we show the D -dependencies of the maximal intensity of the SH radiation in the xz - and yz -planes. For D exceeding $1 \mu\text{m}$, the SH radiation is azimuthally symmetric and the RP represents an empty cone (see inset 1 in the lower row of Figure 2), which is close to the RP of the infinite nonlinear surface [25]—further, we refer to this case as to “no edge case”. For D , in the range of ~ 1 to $\sim 0.5 \mu\text{m}$, the part of the outer obscure ring of $P_z^{2\omega}$ distribution falls over the edge. This causes a little asymmetry between the radiation in the xz - and yz -planes: intensity in the yz -plane slightly rises, whereas in xz -drops. Thus, small lobes in the yz -plane become evident in RP (see inset 2 in the lower row of Figure 2). Further decrease of D causes a significant fraction of the distribution of $P_z^{2\omega}$ (particularly, central bright spot) to fall over the edge. This consequently results in a high asymmetry of the radiation—the SH mostly radiates at the xz -plane and the RP becomes two-lobed (see insets 3 and 4 in the lower row of Figure 2). It is interesting that for $D \sim 0.3 \mu\text{m}$ the magnitude of these lobes even exceeds the magnitude of the RP for “no edge case” shaped as a symmetrical cone. Thus, the effect of the edge of the nonlinear region can increase the SH radiation in a given direction, though, total SH output expectedly drops.

The results of a similar calculation for the linear (x -) polarization of the incoming fundamental wave are presented in Figure 3. In the upper panel of Figure 3, we demonstrate the distribution of $|P_z^{2\omega}|$. Contrary to the radially polarized excitation, the distribution has a minimum in the center. Because of this, a noticeable decrease in the SH intensity occurs for higher values of D (about $0.5 \mu\text{m}$), for which the maximum of $|P_z^{2\omega}|$ mainly falls over the edge. For $D = 0 \mu\text{m}$ (center of the beam is exactly at the edge) maximum of the intensity in the xz -plane, which is the dominant plane of the SH radiation, exhibits about a 4-fold drop, relative to the maximal intensity in “no edge case”. This is expectable, since the SH mostly radiates into two lobes, and we effectively “cut off” half of the nonlinear polarization.

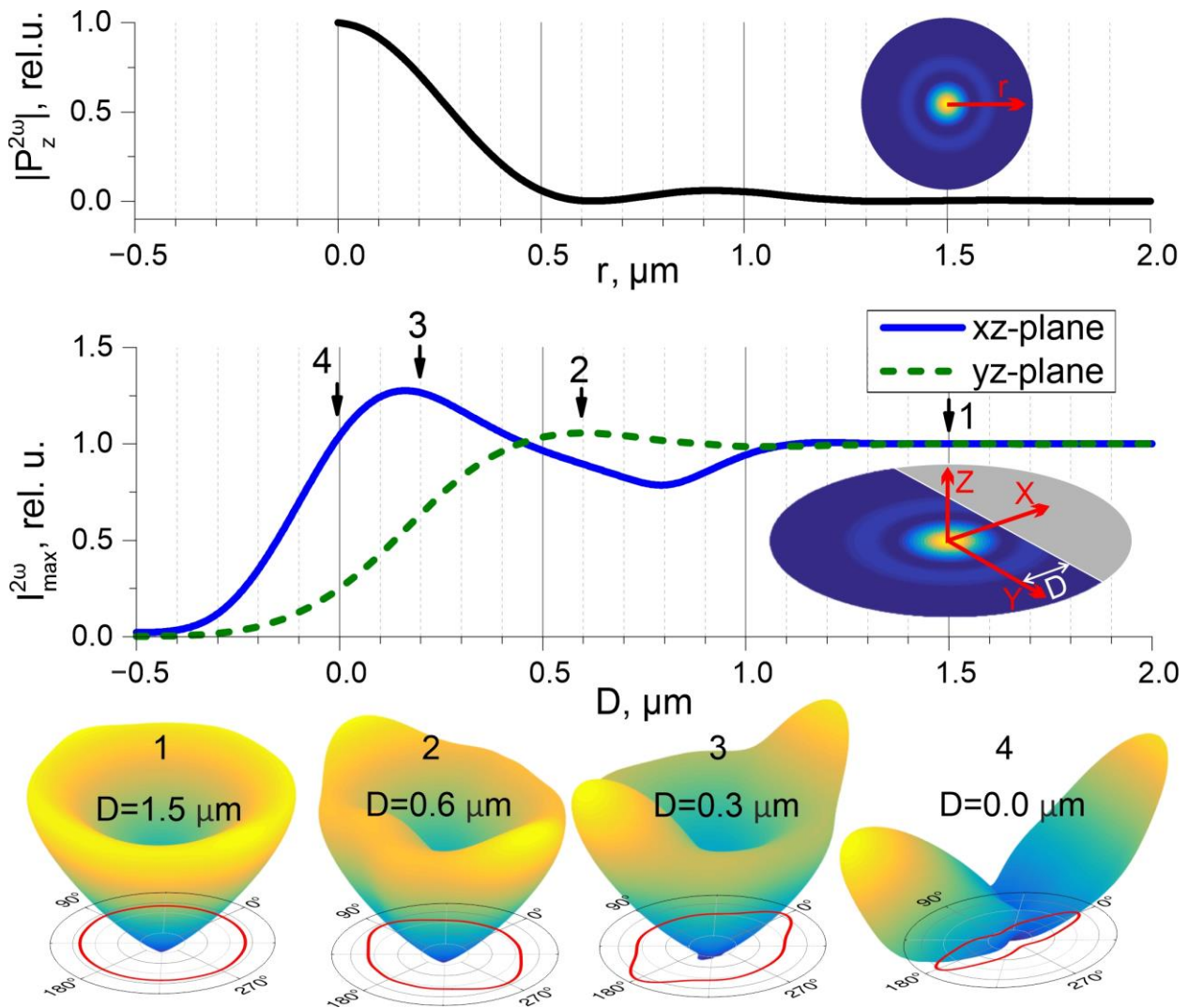


Figure 2. (Upper row): radial distribution of the nonlinear polarization ($|P_z^{2\omega}|$) at the surface possessing $\chi^{(2)}_{zzz}$ -component of second-order susceptibility and excited by a radially polarized beam; inset: 2D-map of the polarization. (Middle row): maxima of the intensity of the SH radiation in xz - (solid curve) and yz -planes (dashed curve) vs. distance between the beam center and the edge of the nonlinear region (D); the axis and D are designated in the inset; negative D corresponds to the beam center falling over the edge. (Lower row): second harmonic radiation patterns for $D = 1.5$ μm (1), $D = 0.6$ μm (2), $D = 0.3$ μm (3), $D = 0.0$ μm (4); contours: maximal SH intensity vs. azimuthal direction.

Interesting to note that for linearly polarized excitation the edge does not greatly change the shape of RP. The two-lobed RP with small side leaflets keeps being two-lobed even in the presence of the edge (see lower panel of Figure 3). This is because the edge does not greatly change the symmetry of the problem: excitation has the dedicated direction (direction of the polarization), and the surface has the preferred direction (direction normal to the edge). For the radially polarized excitation, this change is more drastic (see the lower panel in Figure 2) because the excitation and the surface have different symmetries (cylindrical vs. one with the dedicated lateral direction). Interesting to note that the SH RPs for radial and linear polarized excitations, when the effect of the edge is strong (e.g., for $D = 0$ μm), have a similar two-lobed shape. However, radially polarized light has a more pronounced longitudinal (z -) component of the electric field than the linear one. Estimations made in [25] showed a more than 2-fold difference. This results in about an 8-fold difference of total (integrated over all radiation angles) the SH intensity for $\chi^{(2)}_{zzz}$ -component. Thus,

for $D = 0 \mu\text{m}$, the magnitude of the SH radiation under a radially polarized excitation is tens of times higher than for a linear one (see middle panels in Figures 2 and 3).

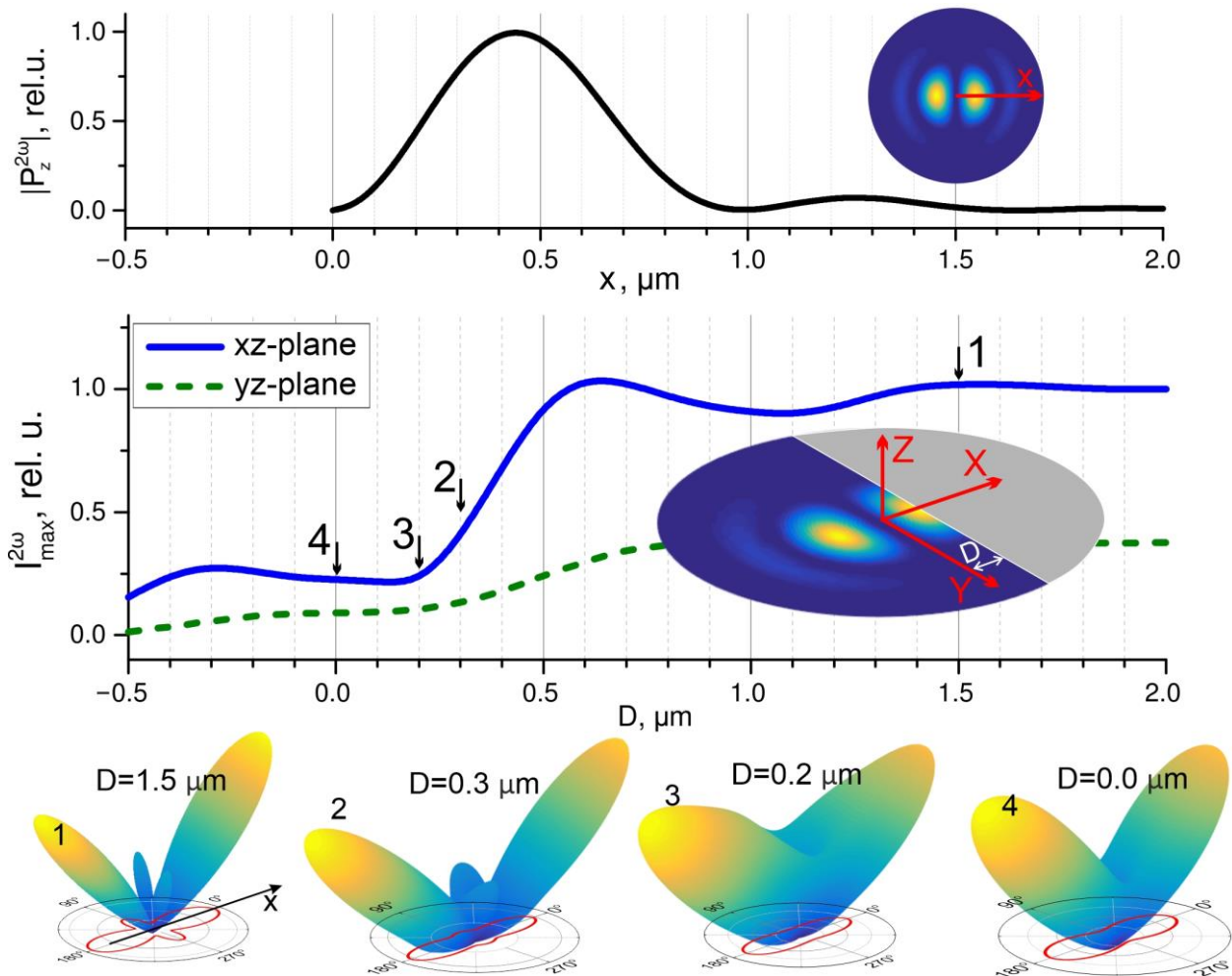


Figure 3. (Upper row): radial distribution of the nonlinear polarization ($|P_z^{2\omega}|$) at the surface possessing $\chi_{zzz}^{(2)}$ -component of the second order susceptibility and excited by a linearly x -polarized beam; inset: 2D-map of the polarization. (Middle row): maxima of the intensity of the SH radiation in xz - (solid curve) and yz -planes (dashed curve) vs. distance between the beam center and the edge of the nonlinear region (D); the axis and D are designated in the inset; negative D corresponds to the beam center falling over the edge. (Lower row): second harmonic radiation patterns for $D = 1.5 \mu\text{m}$ (1), $D = 0.3 \mu\text{m}$ (2), $D = 0.2 \mu\text{m}$ (3), $D = 0.0 \mu\text{m}$ (4); contours: maximal SH intensity vs. azimuthal direction.

3.2. $\chi_{zxx}^{(2)}$ -Component and Normal Radiation

We carried out the same analysis for $\chi_{zxx}^{(2)}$ -component of the second-order susceptibility. This component is responsible for the in-plane component of the nonlinear polarization $\mathbf{P}^{2\omega}$. Therefore, it could provide normal radiation. However, in the case of an infinite nonlinear surface, there is no normal radiation because of the symmetry [25]. Though, when the edge breaks the symmetry of the surface, non-zero radiation in the normal direction should occur. Basically, in “no edge case” there is a highly symmetrical lateral distribution of $\mathbf{P}^{2\omega}$, and radiation in the normal direction is nullified because of destructive interference. In the presence of the edge, though, the condition of destructive interference in the normal direction breaks and corresponding radiation occurs. These reasonings for radially polarized excitation are illustrated in Figure 4. For the linearly polarized excitation, the situation is qualitatively similar.

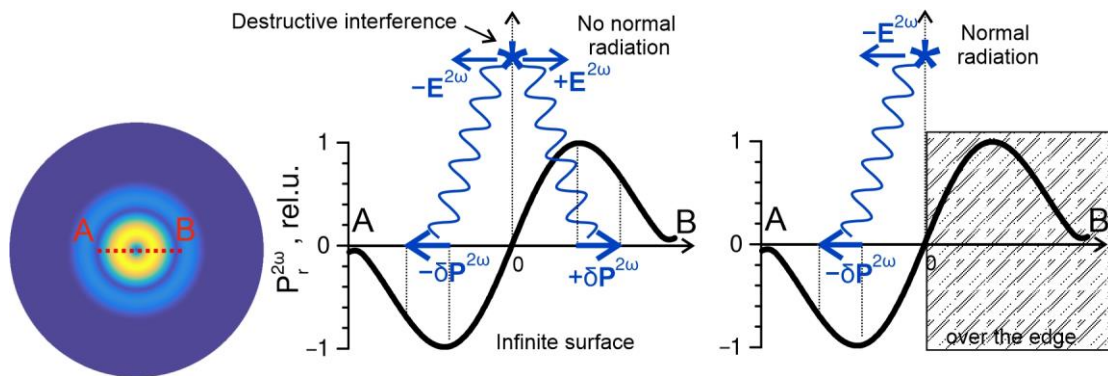


Figure 4. Illustration of the appearance of normal radiation due to the effect of the edge.

In Figure 5, we show the results of calculations for radial polarization of the incoming fundamental wave. The upper panel of Figure 5 demonstrates the radial distribution of $|P_r^{2\omega}|$. The distribution has the shape of two concentric rings, the inner one being about 5-times brighter than the outer one. In the middle panel of Figure 5, we present dependencies of the maximal intensity of the SH radiation in the xz - and yz -planes and the intensity in the normal direction on D . The dependencies of maximal intensities in the two planes are qualitatively similar to the ones demonstrated in Figure 2. Their certain features are related to the features of the $|P_r^{2\omega}|$ -distribution. Here, we omit a detailed description of the dependencies, since it is similar to that in the section regarding $\chi^{(2)}_{zzz}$ -component. Only note that for $D = 0 \mu\text{m}$ the maximal SH intensity in the xz -plane is about a quarter of the value for “no edge case”. This is contrary to the case of $\chi^{(2)}_{zzz}$ -component, where for $D = 0 \mu\text{m}$ the maximal intensity even slightly exceeds the one for “no edge case”.

The most interesting point here is that the edge provides non-zero radiation in the normal direction. In the corresponding dependence represented as a dotted line in the middle panel of Figure 5, we observe two peaks of normal radiation. One (I) is at $\sim 0.6 \mu\text{m}$ —at this distance the outer ring of $|P_r^{2\omega}|$ -distribution falls over the edge. The other (II) is exactly at $D = 0 \mu\text{m}$, when half of the $|P_r^{2\omega}|$ -distribution is over the edge. However, corresponding intensities are about 0.03 and 0.08 of the maximal intensity in “no edge case”. This normal radiation, albeit insignificant, is highly desired since measurements when both exciting and emitting beams are normal to a sample surface can greatly simplify the experiments.

Also, we propose a structure with additional radial confinement of nonlinearity that the “cut off” outer ring of $|P_r^{2\omega}|$ -distribution (see inset 4* in Figure 5, where the corresponding semicircular nonlinear region is drawn). This confinement together with the edge at $D = 0 \mu\text{m}$ provides the relative magnitude of the radiation in the normal direction about ~ 0.3 which is ~ 4 -times higher than the normal radiation without the radial confinement and only 3-times weaker than the maximal intensity. The RP in this case is noticeably elongated in the normal direction (z -) and side lobes are barely seen.

Results for $\chi^{(2)}_{xzx}$ -component and linearly polarized fundamental wave presented in Figure 6, are qualitatively similar to the ones presented in Figure 5. Here, we omit the detailed description and outline only the main characteristics. The major feature is that the surface possessing $\chi^{(2)}_{xzx}$ -component of the second order susceptibility excited by a linearly x -polarized beam for $D = 0 \mu\text{m}$ generates strong SH radiation in the normal direction. The relative magnitude of the normal radiation is 0.5, which is only twice weaker than the magnitude of the SH intensity in “no edge case”. Moreover, the radiation in the normal direction for $D = 0 \mu\text{m}$ is noticeably higher than in other directions. Thus, RP is elongated in this direction (see inset 4 in the lower row of Figure 6). Note, for radially polarized excitation the relative magnitude of the SH intensity in the normal direction was only ~ 0.08 for $D = 0 \mu\text{m}$, and weaker than the magnitude of intensity in the xz -plane.

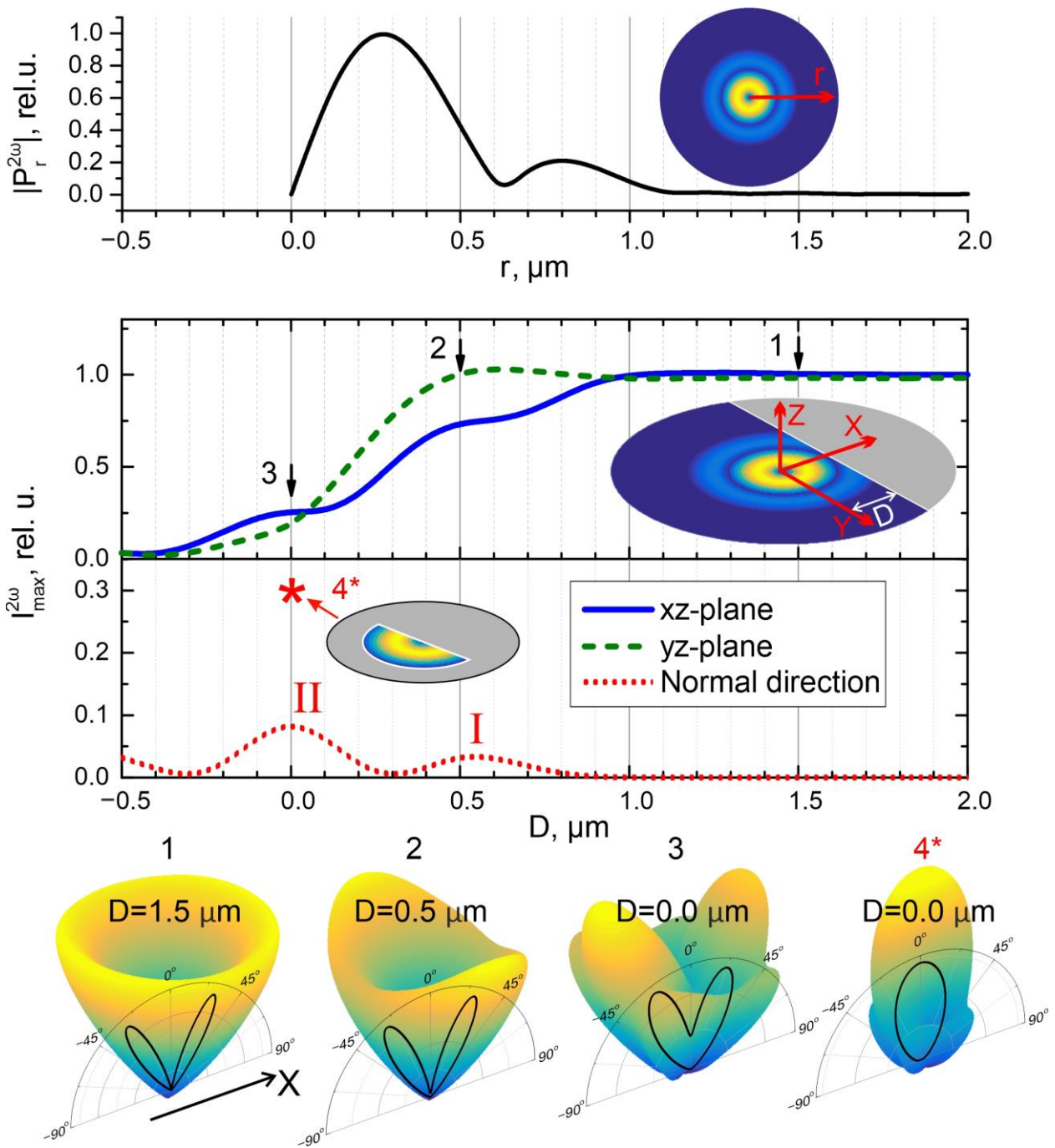


Figure 5. Upper row: radial profile of the distribution of nonlinear polarization ($|P_r^{2\omega}|$) at the surface possessing $\chi_{xz}^{(2)}$ -component of the second order susceptibility and excited by a radially polarized beam; inset: 2D-map of polarization. Middle row: Maxima of the intensity of the SH radiation in xz - (solid curve) and yz -planes (dashed curve) and intensity in the normal direction (dotted curve) vs. distance between the beam center and the edge of the nonlinear region (D); the axis and D are designated in the inset; negative D corresponds to the beam center falling over the edge. Lower row: second harmonic radiation patterns for $D = 1.5 \mu\text{m}$ (1), $D = 0.5 \mu\text{m}$ (2), $D = 0.0 \mu\text{m}$ (3), and $D = 0.0 \mu\text{m}$ (4*) with an addition radial confinement of nonlinearity (see corresponding inset 4*); overlaying curves: cross-sections of RPs in the xz -plane.

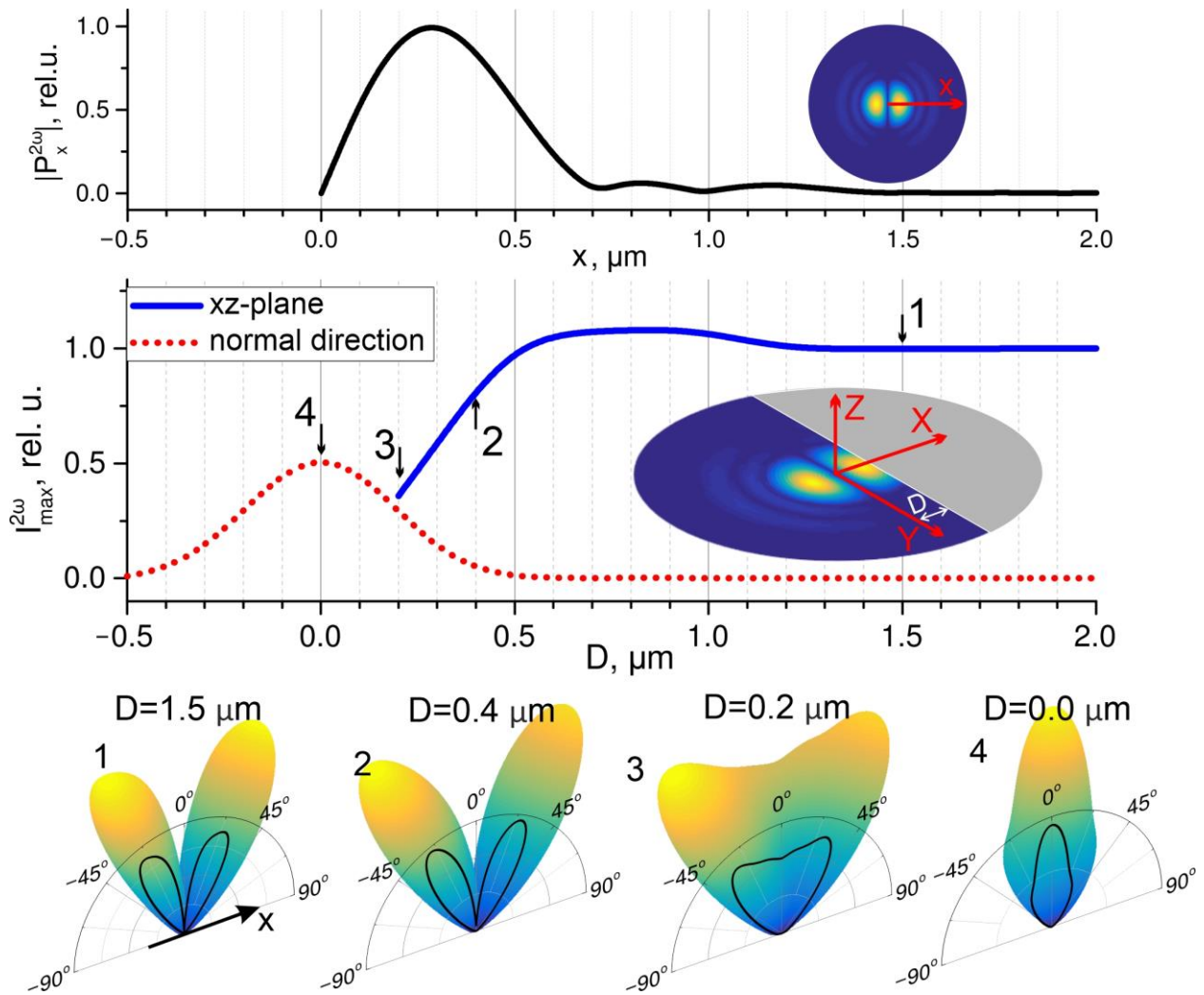


Figure 6. (Upper row): x -profile of distribution of nonlinear polarization ($|P_x^{2\omega}|$) at the surface possessing $\chi_{xzx}^{(2)}$ -component of second-order susceptibility excited by a linearly x -polarized beam; inset: 2D-map of polarization. **(Middle row):** maxima of the intensity of the SH radiation in the xz -plane (solid curve) and the intensity in the normal direction (dotted curve) vs. distance between the beam center and the edge of the nonlinear region (D); the axis and D are designated in the inset; negative D corresponds to the beam center falling over the edge. **(Lower row):** second harmonic radiation patterns for $D = 1.5 \mu\text{m}$ (1), $D = 0.4 \mu\text{m}$ (2), $D = 0.2 \mu\text{m}$ (3) and $D = 0.0 \mu\text{m}$ (4); overlaying curves: cross-sections of RPs in the xz -plane.

To compare the absolute values of the normal radiation for linearly and radially polarized excitations, we normalized magnitudes of fundamental fields so that the integral intensities of the fundamental wave were equal:

$$\int_S |\mathbf{E}_{inc}^{rad}(r, \varphi)|^2 dS = \int_S |\mathbf{E}_{inc}^{lin}(r, \varphi)|^2 dS. \tag{10}$$

Here, \mathbf{E}_{inc}^{rad} and \mathbf{E}_{inc}^{lin} are distributions of the electric field of fundamental radially and linearly polarized waves in the focal plane and the integration is carried out over this plane. Thus, we obtain that the maximum SH intensity for radial polarization for the “no edge case” is ~ 2.2 (in arbitrary units) and for linear polarization ~ 1.4 (in the same arbitrary units). However, for normal radiation for $D = 0 \mu\text{m}$, these values are 0.18 and 0.7, respectively. Thus, normal radiation of the SH for $D = 0 \mu\text{m}$ is about 4-fold more intensive in the case

of the linearly polarized excitation, which makes this configuration very perspective for experiments and applications.

4. Conclusions

We presented a model of surface optical second harmonic generation under tightly focused linearly and radially polarized beams for an arbitrary distribution of the second-order nonlinearity over the surface. Using this model, we analyzed the influence of the straight edge of the nonlinear surface region on the second harmonic radiation patterns. We considered the surface of centrosymmetric media and examined the impacts of $\chi^{(2)}_{zzz}$ and $\chi^{(2)}_{xzx}$ components of the surface second-order susceptibility tensor $\chi^{(2)}$. For $\chi^{(2)}_{zzz}$ -component and radially polarized fundamental wave we demonstrated that the second harmonic radiation pattern transforms from a symmetrical empty cone to a two-lobed diagram as the center of the excitation beam shifts toward the edge of the nonlinear region. The total SH intensity expectedly decreases, however, the intensity in the formed lobes can even exceed the one generated by a surface with uniformly distributed nonlinearity, i.e., the SH radiation becomes more directional. For a linearly polarized fundamental wave, the SH RPs essentially have a two-lobed shape and do not change qualitatively. For $\chi^{(2)}_{xzx}$ -component and both radial and linear polarizations, the influence of the edge leads to the SH radiation in the normal direction. This is a unique result, for the normal SH radiation under the normal excitation is forbidden in commonly used schemes of SHG by surfaces/films. Moreover, we demonstrated that linearly polarized excitation is more effective for the SH radiation in the normal direction (about 4-times for the parameters used) than the radial one. The developed model is also applicable to the SHG by surfaces and thin layers of axially symmetric, C_{4v} and C_{6v} materials.

Author Contributions: Conceptualization, S.S.; Formal analysis, I.R.; Methodology, S.S.; Software, I.R.; Supervision, A.L.; Validation, G.K.; Visualization, G.K.; Writing—original draft, S.S.; Writing—review & editing, A.L. All authors have read and agreed to the published version of the manuscript.

Funding: This research was funded by the Russian Science Foundation, project # 21-72-00048.

Institutional Review Board Statement: Not applicable.

Informed Consent Statement: Not applicable.

Data Availability Statement: No new data were created or analyzed in this study. Data sharing is not applicable to this article.

Conflicts of Interest: The authors declare no conflict of interest.

References

1. Franken, P.A.; Hill, A.E.; Peters, C.W.; Weinreich, G. Generation of optical harmonics. *Phys. Rev. Lett.* **1961**, *7*, 118–119. [[CrossRef](#)]
2. Ren, Y.; Zhao, X.; Hagley, E.W.; Deng, L. Ambient-condition growth of high-pressure phase centrosymmetric crystalline KDP microstructures for optical second harmonic generation. *Sci. Adv.* **2016**, *2*, e1600404. [[CrossRef](#)]
3. Kauranen, M.; Zayats, A.V. Nonlinear plasmonics. *Nat. Photonics* **2012**, *6*, 737–748. [[CrossRef](#)]
4. Liu, T.; Xiao, S.; Li, B.; Gu, M.; Luan, H.; Fang, X. Third- and Second-Harmonic Generation in All-Dielectric Nanostructures: A Mini Review. *Front. Nanotechnol.* **2022**, *4*, 891892. [[CrossRef](#)]
5. Krause, D.; Teplin, C.W.; Rogers, C.T. Optical surface second harmonic measurements of isotropic thin-film metals: Gold, silver, copper, aluminum, and tantalum. *J. Appl. Phys.* **2004**, *96*, 3626–3634. [[CrossRef](#)]
6. Wang, X.; Shen, S.; Sun, J.; Fan, F.; Chang, S. Surface and bulk second-harmonic responses from a glass slide using tightly focused radially polarized light. *Opt. Lett.* **2016**, *41*, 5652–5655. [[CrossRef](#)] [[PubMed](#)]
7. Butet, J.; Russier-Antoine, I.; Jonin, C.; Lascoux, N.; Benichou, E.; Brevet, P.F. Sensing with multipolar second harmonic generation from spherical metallic nanoparticles. *Nano Lett.* **2012**, *12*, 1697–1701. [[CrossRef](#)]
8. Tran, R.J.; Sly, K.L.; Conboy, J.C. Applications of Surface Second Harmonic Generation in Biological Sensing. *Annu. Rev. Anal. Chem.* **2017**, *10*, 387–414. [[CrossRef](#)]
9. Xia, C.; Sun, J.; Wang, Q.; Chen, J.; Wang, T.; Xu, W.; Zhang, H.; Li, Y.; Chang, J.; Shi, Z.; et al. Label-Free Sensing of Biomolecular Adsorption and Desorption Dynamics by Interfacial Second Harmonic Generation. *Biosensors* **2022**, *12*, 1048. [[CrossRef](#)]
10. Wunderlich, S.J. Second Harmonic Light Scattering from Dielectric and Metallic Spherical Nanoparticles. Ph.D. Thesis, Der Friedrich-Alexander-Universität Erlangen-Nürnberg, Erlangen, Germany, 2014.

11. Thyagarajan, K.; Rivier, S.; Lovera, A.; Martin, O.J.F. Enhanced second-harmonic generation from double resonant plasmonic antennae. *Opt. Express* **2012**, *20*, 12860–12865. [[CrossRef](#)]
12. Frizyuk, K.; Volkovskaya, I.; Smirnova, D.; Poddubny, A.; Petrov, M. Second-harmonic generation in Mie-resonant dielectric nanoparticles made of noncentrosymmetric materials. *Phys. Rev. B* **2019**, *99*, 075425. [[CrossRef](#)]
13. Scherbak, S.A.; Lipovskii, A.A. Understanding the Second-Harmonic Generation Enhancement and Behavior in Metal Core–Dielectric Shell Nanoparticles. *J. Phys. Chem. C* **2018**, *122*, 15635–15645. [[CrossRef](#)]
14. Lerman, G.M.; Levy, U. Effect of radial polarization and apodization on spot size under tight focusing conditions. *Opt. Express* **2008**, *16*, 4567–4581. [[CrossRef](#)]
15. Butet, J.; Russier-Antoine, I.; Jonin, C.; Lascoux, N.; Benichou, E.; Brevet, P.-F. Nonlinear Mie theory for the second harmonic generation in metallic nanoshells. *J. Opt. Soc. Am. B* **2012**, *29*, 2213–2221. [[CrossRef](#)]
16. Rodríguez, F.J.; Wang, F.X.; Canfield, B.K.; Cattaneo, S.; Kauranen, M. Multipolar tensor analysis of second-order nonlinear optical response of surface and bulk of glass. *Opt. Express* **2007**, *15*, 8695–8701. [[CrossRef](#)]
17. Scherbak, S.A.; Reshetov, I.V.; Zhurikhina, V.V.; Lipovskii, A.A. Second Harmonic Generation By Surface of Poled Glasses: Modeling and Measurement of Maker Fringes. *St. Petersburg State Polytech. Univ. J. Phys. Math.* **2021**, *14*, 95–113. [[CrossRef](#)]
18. Melik-Gaykazyan, E.V.; Kruk, S.S.; Camacho-Morales, R.; Xu, L.; Rahmani, M.; Zangeneh Kamali, K.; Lamprianidis, A.; Miroschnichenko, A.E.; Fedyanin, A.A.; Neshev, D.N.; et al. Selective Third-Harmonic Generation by Structured Light in Mie-Resonant Nanoparticles. *ACS Photonics* **2018**, *5*, 728–733. [[CrossRef](#)]
19. Bautista, G.; Huttunen, M.J.; Kontio, J.M.; Simonen, J.; Kauranen, M. Third- and second-harmonic generation microscopy of individual metal nanocones using cylindrical vector beams. *Opt. Express* **2013**, *21*, 21918–21923. [[CrossRef](#)]
20. Zhang, W.; Xue, T.; Lu, F.; Zhang, L.; Meng, C.; Wang, J.; Mei, T. Second-order surface optical nonlinear response of plasmonic tip axially excited via ultrafast vector beams. *Appl. Phys. Express* **2020**, *13*, 032002. [[CrossRef](#)]
21. Biss, D.P.; Brown, T.G. Polarization-vortex-driven second-harmonic generation. *Opt. Lett.* **2003**, *28*, 923–925. [[CrossRef](#)]
22. Ohtsu, A. Second-harmonic wave induced by vortex beams with radial and azimuthal polarizations. *Opt. Commun.* **2010**, *283*, 3831–3837. [[CrossRef](#)]
23. Pakhomov, A.V.; Löchner, F.J.F.; Zschiedrich, L.; Saravi, S.; Hammerschmidt, M.; Burger, S.; Pertsch, T.; Setzpfandt, F. Far-field polarization signatures of surface optical nonlinearity in noncentrosymmetric semiconductors. *Sci. Rep.* **2020**, *10*, 10545. [[CrossRef](#)]
24. Sun, J.; Wang, X.; Chang, S.; Zeng, M.; Shen, S.; Zhang, N. Far-field radiation patterns of second harmonic generation from gold nanoparticles under tightly focused illumination. *Opt. Express* **2016**, *24*, 7477–7487. [[CrossRef](#)] [[PubMed](#)]
25. Scherbak, S.A.; Lipovskii, A.A. Optical second-harmonic response of axially symmetric media under tightly focused excitation: Linear versus radial polarization. *J. Opt. Soc. Am. B* **2022**, *39*, 2237–2245. [[CrossRef](#)]
26. An, H.; Fleming, S. Second-order optical nonlinearity and accompanying near-surface structural modifications in thermally poled soda-lime silicate glasses. *J. Opt. Soc. Am. B* **2006**, *23*, 2303–2309. [[CrossRef](#)]
27. Chervinskii, S.; Sevriuk, V.; Reduto, I.; Lipovskii, A. Formation and 2D-patterning of silver nanoisland film using thermal poling and out-diffusion from glass. *J. Appl. Phys.* **2013**, *114*, 224301. [[CrossRef](#)]
28. Fleming, L.A.H.; Goldie, D.M.; Abdolvand, A. Imprinting of glass. *Opt. Mater. Express* **2015**, *5*, 1674–1681. [[CrossRef](#)]
29. Dussauze, M.; Rodriguez, V.; Adamietz, F.; Yang, G.; Bondu, F.; Lepicard, A.; Chafer, M.; Cardinal, T.; Fargin, E. Accurate Second Harmonic Generation Microimprinting in Glassy Oxide Materials. *Adv. Opt. Mater.* **2016**, *4*, 929–935. [[CrossRef](#)]
30. Dadap, J.I.; Shan, J.; Heinz, T.F. Theory of optical second-harmonic generation from a sphere of centrosymmetric material: Small-particle limit. *J. Opt. Soc. Am. B* **2004**, *21*, 1328–1347. [[CrossRef](#)]
31. Hermans, A.; Kieninger, C.; Koskinen, K.; Wickberg, A.; Solano, E.; Dendooven, J.; Kauranen, M.; Clemmen, S.; Wegener, M.; Koos, C.; et al. On the determination of $\chi(2)$ in thin films: A comparison of one-beam second-harmonic generation measurement methodologies. *Sci. Rep.* **2017**, *7*, 44581. [[CrossRef](#)]
32. Drevinskas, R.; Zhang, J.; Beresna, M.; Gecevičius, M.; Kazanskii, A.G.; Svirko, Y.P.; Kazansky, P.G. Laser material processing with tightly focused cylindrical vector beams. *Appl. Phys. Lett.* **2016**, *108*, 221107. [[CrossRef](#)]
33. Biss, D.P.; Brown, T.G. Cylindrical vector beam focusing through a dielectric interface. *Opt. Express* **2001**, *9*, 490–497. [[CrossRef](#)] [[PubMed](#)]
34. Richards, B.; Wolf, E. Electromagnetic diffraction in optical systems, II. Structure of the image field in an aplanatic system. *Proc. R. Soc. London. Ser. A. Math. Phys. Sci.* **1959**, *253*, 358–379. [[CrossRef](#)]

Disclaimer/Publisher’s Note: The statements, opinions and data contained in all publications are solely those of the individual author(s) and contributor(s) and not of MDPI and/or the editor(s). MDPI and/or the editor(s) disclaim responsibility for any injury to people or property resulting from any ideas, methods, instructions or products referred to in the content.